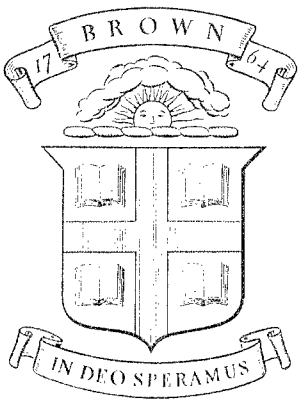

Division of Engineering
BROWN UNIVERSITY
PROVIDENCE, R. I.

AN ANALYSIS OF THE TRIAXIAL TEST FOR COHESIONLESS SOILS

P. R. PASLAY and J. B. WEIDLER

Department of Defense
Advanced Research Projects Agency
Contract SD-86
Materials Research Program

ARPA E41

May 1967

AN ANALYSIS OF THE TRIAXIAL TEST FOR COHESIONLESS SOILS

by

Paul R. Paslay and Jay B. Weidler

Division of Engineering
Brown University
Providence, Rhode Island

May, 1967

ARPA SD-86
Report E 41, May 1967
An Analysis of the Triaxial Test for Cohesionless Soils, P. R. Paslay and J. B. Weidler

Errata: (June 1967)

1. Page 13: Equation (35) should read

$$\dot{\sigma}_C = -2\left[\frac{\sin\phi}{1-\sin\phi}\cdot\frac{\partial c}{\partial v} + (c-\sigma_L)\frac{\cos\phi}{(1-\sin\phi)^2}\frac{\partial\phi}{\partial v}\right]\dot{v}$$

2. Page 15: Equation (44) should read

$$S^{**} = S^{**}(v, \sigma_L)$$

$$= \frac{Z}{H}\cdot\frac{v.\cos2\psi}{\cos\psi}\left[-2\left\{\frac{\sin\phi}{1-\sin\phi}\cdot\frac{\partial c}{\partial v} + (c-\sigma_L)\frac{\cos\phi}{(1-\sin\phi)^2}\frac{\partial\phi}{\partial v}\right\}\right.$$

$$-\left\{\frac{\tan3\psi}{\sin2\psi}\cdot\frac{(c-\sigma_L)\sin\phi}{}\right\}\cdot\left\{\left(\frac{\cos\phi\,[3G-2+G\cos2\psi]}{2-G\,[1+\sin\phi]}\right)\frac{\partial\phi}{\partial v}\right.$$

$$+\left(\frac{[1+\sin\phi][3+\cos2\psi]}{2-G\,[1+\sin\phi]}\right)\left(\frac{\partial G}{\partial v} - \frac{2}{3}\frac{\partial G}{\partial\sigma}\left[\frac{\sin\phi}{1-\sin\phi}\frac{\partial c}{\partial v}\right.\right.$$

$$\left.\left.\left.+\frac{\{c-\sigma_L\}\cos\phi}{\{1-\sin\phi\}^2}\frac{\partial\phi}{\partial v}\right]\right)\right\}\Bigg]$$

3. Page 18: The units of Equation (52.c) should be

lb.-in./lb.

4. Page 19: Equation (56.b) should read

$$\dot{v} = -17.48\,\frac{\dot{Z}}{H}$$

5. Page 19: Equation (58.g) should read

$$\frac{\dot{Y}}{H} = -1.755\,\frac{\dot{Z}}{H}$$

6. Page 32: Equation (32) should read

$$\dot{Y} = -(\tan\psi)\,\dot{Z}$$

AN ANALYSIS OF THE TRIAXIAL TEST FOR COHESIONLESS SOILS*

by

Paul R. Paslay** and Jay B. Weidler***

Several implications of an earlier analytical formulation for cohesionless soils are deduced for the triaxial test (a compression test in the presence of a hydrostatic pressure). A specific form for the loading surface is adopted in order to illustrate certain difficulties associated with uniqueness and stability. In certain important respects the limited analytical and numerical results appear to agree with experience in soil mechanics testing.

---

* The research reported here was supported by ARPA Contract E-47.

** Professor of Engineering, Brown University.

*** Assistant Professor of Engineering (Research), Brown University.

Introduction

In a previous report [1]* the authors proposed an analytical formulation for the prediction of isothermal flow of an idealized cohesionless soil subjected to mechanical load. The material was assumed to be time-independent, isotropic, and rigid-plastic. Although, in a broad sense, the formulation adequately represents certain aspects of the deformation characteristics of the soil, the generality of the formulation must be reduced to a specific relationship which can be compared with experience and experimental results.

Such a relationship not only is useful in verifying the analytical formulation but also provides a means for evaluating certain experimental considerations. In the triaxial test, for example, it becomes possible to assess the influence of the details of the loading system, the influence of the membrane which encloses the sample, or the interplay between a continously distributed strain field and the presence of slip planes on which the shearing concentrates.

The work presented here is an attempt to study some of the implications of the earlier analytical formulation for the specific case of a triaxial test. This is accomplished by assuming a definite function to describe the loading surface and applying it to a triaxial test on an initially homogeneous soil sample. This test is currently the most widely used experimental technique for evaluating soil response.

The next section indicates the specific choice of the loading surface adopted in this investigation and the stress-deformation rate

---

* Numbers in brackets designate references listed in the bibliography.

relations associated with it. Subsequent sections deal with questions of stability and uniqueness, and the superposition, onto a constant hydrostatic pressure, of a compression test which is the triaxial test. Finally calculated results are given for a specific case which indicate that this formulation is capable of predicting the type of flow which is observed in practice.

Analytical Formulation

As mentioned earlier the material under consideration is assumed to be isotropic, initially homogeneous and to exhibit rigid-plastic, time independent, isothermal behavior. The loading surface chosen is a Coulomb-Mohr type which closes, in some manner, at sufficiently high hydrostatic pressure. Figure 1 shows the Coulomb-Mohr surface in principal stress space. A cross section of this surface perpendicular to the vector $\vec{i} + \vec{j} + \vec{k}$ is of interest. The plane of this cross section is referred to as the π plane and is shown in Figure 2 with the notation

$$\sigma = \frac{1}{3}(\sigma_1 + \sigma_2 + \sigma_3) \tag{1}$$

It is noted that in the ensuing development tensile stresses are taken as positive. Figures 1 and 2 are derived [2] by hypothesizing that deformation is initiated if the following function, considering every plane through a point,

$$\frac{|\text{resolved shear stress}|}{-\text{normal stress} + c} \tag{2}$$

reaches a critical value denoted by $\tan \phi$. In other words, if considering all planes through the point in question, the function (2) attains the value $\tan \phi$ on one plane or simultaneously or more than one plane, i.e.

$$\left.\frac{|\text{resolved shear stress}|}{-\text{normal stress} + c}\right|_{\max} = \tan \phi \tag{3}$$

then the associated stress state is on the loading surface.

Clearly, for the Coulomb-Mohr material, c and ϕ are the two material parameters which determine the loading surface. It has been suggested [3] that such a loading surface is only valid for sufficiently small values of $-\sigma$ and that for larger values the surface closes. Figure 3 shows a section of σ_1, σ_2, σ_3 space which includes the σ_3 axis and is parallel to the vector $\vec{i} + \vec{j} + \vec{k}$. The dotted line in this figure is the type of "cut-off" of the Coulomb-Mohr surface which is envisioned in this work. The subsequent analytical development is now restricted to be for stress states on the Coulomb-Mohr portion of the loading surface. In this way the details of the dotted part of the yield surface in Figure 3 may be ignored.

In this paper the symbol U will represent the internal energy per unit mass of the soil. It is noted that in reference [1], U represented the internal energy per unit current volume. As in [1] U is taken to be a function of the specific volume, v. Then following the usual reasoning that the deformation rate, denoted by its principal values d_1, d_2, d_3 and expressed in terms of the vector $d_1\vec{i} + d_2\vec{j} + d_3\vec{k}$, is determined or delimited by the location of the stress point σ_1, σ_2, σ_3 on the loading surface, restrictions on the direction of $d_1\vec{i} + d_2\vec{j} + d_3\vec{k}$, may be deduced from energy considerations. Due to the presence of U(v) the often employed normality condition [4] is not directly determined. Instead, the acceptable directions for $d_1\vec{i} + d_2\vec{j} + d_3\vec{k}$, are found to be included in a "fan" of directions at each point. In order to predict specific results it is necessary to chose a direction for $d_1\vec{i} + d_2\vec{j} + d_3\vec{k}$. If the compression test superimposed on a hydrostatic pressure is to be considered a further complication arises in that the stress point is on an edge of the loading surface. The deformation rate chosen here which is acceptable according to the previously mentioned derivation [1] is the sum of a vector normal to the loading surface and a vector parallel to $\vec{i} + \vec{j} + \vec{k}$. As the normal to the

loading surface at an edge is not uniquely determined a linear combination of two vectors is determined for this point. Figure 4 shows the details of the construction. In this case the deformation rate vector for a triaxial test may then be represented by

$$d_1 = -(\Lambda_1 + \Lambda_3)\left(\frac{1 - \sin\phi}{1 + \sin\phi} + G\right) \tag{4a}$$

$$d_2 = +\Lambda_1 (1 - G) + \Lambda_2 (-G) \tag{4b}$$

$$d_3 = +\Lambda_1 (-G) + \Lambda_2 (1 - G) \tag{4c}$$

where Λ_1 and Λ_2 are arbitrary positive numbers and

$$G = \alpha \frac{\partial U}{\partial v} \cdot \frac{2 \sin\phi}{3(1 + \sin\phi)(\sigma_o - \sigma + \alpha \frac{\partial U}{\partial v})} \tag{5}$$

It should be noted that when G vanishes the $d_1\vec{i} + d_2\vec{j} + d_3\vec{k}$ vector lies in a plane perpendicular to the edge of the loading surface. The advantage of the formulation for G in Equation (5) is that as σ approaches σ_o for points on the loading surface the deformation rate vector approaches being parallel to the π plane (i.e. - approaches constant volume flow). This is consistent with experience in soil mechanics.

Finally for a soil, similar to a metal, the yield surface changes as the deformation ensues. The most important variable controlling the changes appears to be the specific volume so that in the following it is assumed that the material parameters c, ϕ, σ_o, and U are each function of v. Restrictions on the behavior of these parameters are given in Equations (6) below. Although the physical significance of these parameters has been indicated in Figures 1 through 4 a brief discussion of them is included for clarity. The parameter c(v) is a measure of the cohesive strength of the material which for truly cohesionless soils (i.e. dry sand grains) may be assumed equal to zero. ϕ(v)

is often called the angle of internal friction of the material and in this work serves as a measure of the linear rate at which the Coulomb-Mohr surface diverges from the hydrostatic axis with increasing hydrostatic pressure. The function σ_o (v) represents the spherical portion of a stress tensor on the loading surface which would induce constant volume flow. Finally the parameter U(v) is the internal energy per unit mass.

The following restrictions on the behavior of these parameters appear to be physically appropriate

$$c(v) \geq 0 \tag{6a}$$

$$\frac{\partial c}{\partial v} \leq 0 \tag{6b}$$

$$0 \leq \phi(v) \leq \pi/2 \tag{6c}$$

$$\frac{\partial \phi}{\partial v} \leq 0 \tag{6d}$$

$$\sigma_o < \frac{\partial U}{\partial v} \leq 0 \tag{6e}$$

$$\frac{\partial \sigma_o}{\partial v} \geq 0 \tag{6f}$$

$$\left| \frac{\partial U}{\partial v} \right| << \left| \sigma_o \right| \tag{6g}$$

The last of these restrictions coupled with restriction (6e) indicates that even though internal energy may be returned to the system during plastic work with increasing specific volume, its rate of return with respect to the increasing specific volume is small compared to σ_o. That portion of $\frac{\partial U}{\partial v}$ which is available to assist the superimposed stresses in doing plastic work while inducing a differential change of plastic strain is denoted by $\alpha \frac{\partial U}{\partial v}$ where α, a material parameter, is restricted to $0 < \alpha < 1$.

Uniqueness and Stability

It has been previously shown [5] that normality of the deformation

rate vector to the yield surface must exist to ensure certain uniqueness properties. Since normality is not satisfied here a general lack of uniqueness is to be expected. The question arises then as to how the actual solution can be selected from all those deduced by the theory. That such a selection should be possible is a result of the observation that experiments in soil mechanics are repeatable. What is desired, then, is a means of selecting from the predicted solutions that one which will occur in an experiment. In this investigation of the triaxial test a lack of uniqueness of the flow field is shown and the actual field must be chosen.

The criterion which will be used to discriminate between solutions is determined from the way in which the rate of work changes during a prescribed flow. Suppose that the external loading necessary to initiate the flow has a distribution represented by $\vec{F}$ and that the associated velocity field is represented by $\dot{\vec{X}}$. Now for certain parts of the flow field (e.g. possibly part of the boundary) the $\dot{\vec{X}}$ vector is prescribed as a function of time. After the first interval of loading during a time interval Δt the displacements are, to first order terms in Δt, $\dot{\vec{X}}\Delta t$. During this period the loading distribution is changed to $\vec{F} + \vec{F}\Delta t$. Consider the quantity

$$\frac{d}{dt} \int_{\text{system}} \vec{F} \cdot \dot{\vec{X}} \qquad (7)$$

which is the time rate of change of doing work on the system. For each solution deduced from the theory, Expression (7) can be evaluated. It is hypothesized here that of all the possible solutions the one which minimizes Expression (7) is the actual one.

Triaxial Test of an Initially Homogeneous Sample

Figure 5 shows a sketch of the usual triaxial test. σ_L represents the hydrostatic pressure which is assumed to be applied initially and maintained at a constant predetermined value. For soils σ_L is usually a negative number. Subsequently a compressive stress, $-\sigma_C$, is applied to the homogeneous sample until deformation occurs. In this case take

$$\sigma_1 = \sigma_C + \sigma_L \tag{8a}$$

$$\sigma_3 = \sigma_2 = \sigma_L \tag{8b}$$

From Figure 2 these stresses are substituted into the stress state corresponding to point A with the result that the value of σ_C required to initiate flow is

$$\sigma_C = -2(c - \sigma_L)\ \frac{\sin\phi}{1 - \sin\phi} \tag{9}$$

The deformation rates associated with this stress state are now investigated. Two separate solutions will be presented and examined. Alternatively a linear combination of the two solutions could be investigated with the same result. In any event the deformation rates are deduced from Equations (4) to be

$$d_z = d_1 = -(\Lambda_1 + \Lambda_2)\left(\frac{1 - \sin\phi}{1 + \sin\phi} + G\right) \tag{10a}$$

$$d_y = d_2 = \Lambda_1 (1 - G) + \Lambda_2(-G) \tag{10b}$$

$$d_x = d_3 = \Lambda_1 (-G) + \Lambda_2(1 - G) \tag{10c}$$

The uniform height of the sample is reduced now at a constant rate $\dot{Z}$ and the resulting flow field is to be determined.

First the case of homogeneous deformation of the sample with symmetry about the z axis will be considered. In this case d_x and d_y are equal so that from the Equations (10.b and 10.c)

$$\Lambda_1 = \Lambda_2 > 0 \tag{11}$$

and Equation (10.2) becomes

$$d_z = -2\Lambda_1 \left(\frac{1 - \sin\phi}{1 + \sin\phi} + G \right) \tag{12}$$

Now rather than use Λ_1 it is more convenient to work in terms of the constant $\dot{Z}$. Since d_z equals, in this case, $\frac{\dot{Z}}{Z}$, Equation (12) yields

$$\Lambda_1 = -\frac{1}{2} \left(\frac{\dot{Z}}{Z} \right) \left(\frac{1 + \sin\phi}{1 - \sin\phi + G\,[1 + \sin\phi]} \right) \tag{13}$$

Now applying Equations (11) and (13) to Equations (10) gives

$$d_z = \frac{\dot{Z}}{Z} \tag{14a}$$

$$d_x = d_y = -\frac{1}{2} \left[\frac{(1 + \sin\phi)\,(1 - 2G)}{1 - \sin\phi + G\,(1 + \sin\phi)} \right] \left(\frac{\dot{Z}}{Z} \right) \tag{14b}$$

In order to evaluate Equation (7) note that

$$\int_{\text{system}} \vec{F} \cdot \vec{\dot{X}} = (\sigma_C + \sigma_L)\,\pi R^2 \dot{Z} + \sigma_L 2\pi R Z \dot{R} \tag{15}$$

Recalling that $\dot{Z}$ and σ_L are constant, Equation (15) yields

$$\frac{d}{dt} \left(\int_{\text{system}} \vec{F} \cdot \vec{\dot{X}} \right) = \sigma_C \pi R^2 \ddot{Z} + (\sigma_C + \sigma_L)\, 2\pi R \dot{R} \dot{Z} + \sigma_L 2\pi Z (\dot{R}^2 + R\ddot{R}) \tag{16}$$

The evaluation of $\dot{\sigma}_C$ is accomplished by differentiating σ_C in Equation (9)

$$\dot{\sigma}_C = -2 \left[\left(\frac{\sin\phi}{1 - \sin\phi} \right) \frac{\partial c}{\partial v} + \frac{(c - \sigma_L)\cos\phi}{(1 - \sin\phi)^2} \frac{\partial \phi}{\partial v} \right] \dot{v} \tag{17}$$

Now $\dot{v}$ is determined as follows

$$\dot{v} = (d_x + d_y + d_z)\, v = -\left[\frac{2\sin\phi - 3G\,(1 + \sin\phi)}{1 - \sin\phi + G\,(1 + \sin\phi)} \right] \left(\frac{\dot{Z}}{Z} \right) v \tag{18}$$

The quantity $\dot{R}$ is determined by noting that d_x for this case is equal to $(\dot{R}/R)$ which from Equation (14.b) becomes

$$\dot{R} = -\frac{1}{2}\left[\frac{(1+\sin\phi)(1-2G)}{1-\sin\phi+G\,(1+\sin\phi)}\right] R \cdot \frac{\dot{Z}}{Z} \tag{19}$$

Differentiation with respect to time of Equation (19) gives for $\ddot{R}$

$$\ddot{R} = -\frac{1}{2} R \left(\frac{\dot{Z}}{Z}\right)\left[\left\{\frac{(1+\sin\phi)(1-2G)}{1-\sin\phi+G\,(1+\sin\phi)}\right\}\left\{\left(\frac{\dot{R}}{R}\right)-\left(\frac{\dot{Z}}{Z}\right)\right\}\right.$$

$$+\dot{v}\left\{\frac{2\,(1-2G)\cos\phi\,\frac{\partial\phi}{\partial v}-(1+\sin\phi)(3-\sin\phi)\,\frac{\partial G}{\partial v}}{(1-\sin\phi+G\,[1+\sin\phi])^2}\right\}$$

$$\left.-\frac{\dot{\sigma}_c}{3}\left\{\frac{(1+\sin\phi)(3-\sin\phi)\,\frac{\partial G}{\partial\sigma}}{(1-\sin\phi+G\,[1+\sin\phi])^2}\right\}\right] \tag{20}$$

Now Equations (9), (17), (19) and (20) may be used to eliminate σ_c, $\dot{\sigma}_c$, $\dot{R}$, and $\ddot{R}$ from Equation (16). Subsequent to the operation eliminate $\dot{v}$ with Equation (18). The result may be expressed as

$$\frac{d}{dt}\left(\int_{\text{system}} \vec{F} \cdot \dot{\vec{X}}\right) = \pi R^2 Z \left(\frac{\dot{Z}}{Z}\right)^2 S^* \tag{21}$$

where

$$S^* = S^*(\sigma_L, v)$$

$$= +2\left[\left\{\frac{(c-\sigma_L)\cos\phi}{(1-\sin\phi)^2}\,\frac{\partial\phi}{\partial v}+\frac{\sin\phi}{1-\sin\phi}\,\frac{\partial c}{\partial v}\right\}\cdot\right.$$

$$\left.\left\{\frac{2\sin\phi-3G\,(1+\sin\phi)}{(1-\sin\phi)+G\,(1+\sin\phi)}\right\}\right] v + 2(c-\sigma_L)\left[\left\{\frac{\sin\phi}{1-\sin\phi}\right\}\cdot\right.$$

$$\left.\left\{\frac{(1+\sin\phi)(1-2G)}{1-\sin\phi+G\,(1+\sin\phi)}\right\}\right] + \sigma_L\left[-2\left\{\frac{(1+\sin\phi)(1-2G)}{1-\sin\phi+G\,(1+\sin\phi)}\right\}\right.$$

$$+\frac{1}{2}\left\{\frac{(1+\sin\phi)(1-2G)}{1-\sin\phi+G\,(1+\sin\phi)}\right\}^2 + \left\{\frac{(1+\sin\phi)(1-2G)}{1-\sin\phi+G\,(1+\sin\phi)}\right\}\cdot$$

$$\left\{1+\frac{1}{2}\,\frac{(1+\sin\phi)(1-2G)}{1-\sin\phi+G\,(1+\sin\phi)}\right\} + \left\{\frac{2\sin\phi-3G\,(1+\sin\phi)}{1-\sin\phi+G\,(1+\sin\phi}\right\}\cdot v\cdot$$

$$\left\{\frac{2\,(1-2G)\cos\phi\,\dfrac{\partial\phi}{\partial v}-(1+\sin\phi)(3-\sin\phi)\,\dfrac{\partial G}{\partial v}}{(1-\sin\phi+G\,[1+\sin\phi])^2}\right.$$

$$+\frac{2}{3}\left\{\frac{(c-\sigma_L)\cos\phi}{(1-\sin\phi)^2}\,\frac{\partial\phi}{\partial v}+\frac{\sin\phi}{1-\sin\phi}\,\frac{\partial c}{\partial v}\right\}\cdot\left\{\frac{2\sin\phi-3G\,(1+\sin\phi)}{1-\sin\phi+G\,(1+\sin\phi)}\right\}$$

$$\left.\cdot\, v\cdot\left\{\frac{(1+\sin\phi)(3-\sin\phi)\,\dfrac{\partial G}{\partial\sigma}}{(1-\sin\phi+G\,[1+\sin\phi])^2}\right\}\right] \qquad (22)$$

S^* may be regarded as a function, for a specific material, of v and σ_L since ϕ, c, U, σ_o and consequently through Equation (5), G are considered to be specified functions of v. When $S^*(\sigma_L, v)$ is negative then the system is unstable in the sense of [5].

For the second deformation solution of the triaxial test a combination of shear and lateral expansion of an inclined layer of the material is considered. The thickness of the layer is taken as H. Figure 6a indicates a plane parallel to the layer and Figure 6b indicates the deformation state after a small amount of motion. The velocity field with components $\dot{u}_\eta$, $\dot{u}_\xi$, $\dot{u}_\zeta$ in the deforming region may be expressed by

$$\dot{u}_\eta = \frac{V_\eta}{H}\,\xi \qquad (23.a)$$

$$\dot{u}_\xi = \frac{V_\xi}{H}\,\xi \qquad (23.b)$$

$$\dot{u}_\zeta = 0 \qquad (23.c)$$

V_η and V_ξ are velocity components of the upper rigid part of the sample shown in Figure 6b which undergoes a rigid body translation. The velocity components

$\dot{Z}$ and $\dot{Y}$ are related to V_η and V_ξ as follows

$$\dot{Z} = V_\xi \cos\psi - V_\eta \sin\psi \tag{24.a}$$

$$\dot{Y} = V_\xi \sin\psi + V_\eta \cos\psi \tag{24.b}$$

For this motion the components of the deformation rate tensor in the deforming region are

$$d_{\xi\xi} = \frac{1}{H} V_\xi \tag{25.a}$$

$$d_{\eta\eta} = 0 \tag{25.b}$$

$$d_{\zeta\zeta} = 0 \tag{25.c}$$

$$d_{\xi\eta} = \frac{1}{2H} V_\xi \tag{25.d}$$

$$d_{\eta\zeta} = 0 \tag{25.e}$$

$$d_{\zeta\xi} = 0 \tag{25.f}$$

To determine how these deformation rate components may be matched with those given by Equations (10) it is noted that the ζ and x axes are coincident, thus d_x must also vanish and this requirement leads to

$$\Lambda_2 = \frac{G}{1 - G} \Lambda_1 \tag{26}$$

The principal deformation rate components may then be expressed as

$$d_x = 0 \tag{27.a}$$

$$d_y = \Lambda_1 \left(\frac{1 - 2G}{1 + G}\right) \tag{27.b}$$

$$d_z = -\Lambda_1 \left(\frac{1}{1 - G}\right)\left(\frac{1 - \sin\phi}{1 + \sin\phi} + G\right) \tag{27.c}$$

Now the angle ψ in Figure 6 is determined from the condition that $d_{\eta\eta}$ be zero. The Mohr strain circle for this case is shown in Figure 7. In order for $d_{\eta\eta}$ to vanish it may be deduced from the circle that

$$\cos 2\psi = \frac{-2 \sin\phi + 3G (1 + \sin\phi)}{2 - G (1 + \sin\phi)} \tag{28}$$

and also that

$$d_{\xi\xi} = \Lambda_1 \frac{1}{1 - G} \left[\frac{2 \sin\phi - 3G (1 + \sin\phi)}{1 + \sin\phi}\right] \tag{29.a}$$

$$d_{\eta\xi} = \Lambda_1 \frac{1}{1 - G} \left[\frac{1 - (G/2)(1 + \sin\phi)}{1 + \sin\phi}\right] \sin 2\psi \tag{29.b}$$

Combining this result with Equations (25) gives

$$V_{\xi} = \Lambda_1 \frac{H}{1 - G} \left[\frac{2 \sin\phi - 3G (1 + \sin\phi)}{1 + \sin\phi}\right] \tag{30.a}$$

$$V_{\eta} = \Lambda_1 \frac{2H}{1 - G} \left[\frac{1 - (G/2)(1 + \sin\phi)}{1 + \sin\phi}\right] \tag{30.b}$$

and introducing Equations (30) into Equations (24) yields

$$\dot{Z} = \Lambda_1 \frac{H}{1 - G} \left[\left\{\frac{2 \sin\phi - 3G (1 + \sin\phi)}{1 + \sin\phi}\right\} \cos\psi - \left\{\frac{2 - G (1 + \sin\phi)}{1 + \sin\phi}\right\} \sin 2\psi \sin\psi\right] \tag{31.a}$$

$$\dot{Y} = \Lambda_1 \frac{H}{1 - G} \left[\left\{\frac{2 \sin\phi - 3G (1 + \sin\phi)}{1 + \sin\phi}\right\} \sin\psi + \left\{\frac{2 - G (1 + \sin\phi)}{1 + \sin\phi}\right\} \sin 2\psi \cos\psi\right] \tag{31.b}$$

Expressing $\dot{Y}$ as a function of $\dot{Z}$ by use of Equations (31) gives after some manipulation

$$\dot{Y} = (\tan 3\psi)\dot{Z} \tag{32}$$

Finally the rate of change of specific volume, defined by $(d_x + d_y + d_z)\, v$, is

$$\dot{v} = \frac{v. \cos 2\psi}{\cos\psi} \cdot \frac{\dot{Z}}{H} \tag{33}$$

The stress state change is more complex for this motion than it was for the first deformation mode considered. In the present case the principal stress directions rotate once motion begins and this must be accounted for in determining

$\frac{d}{dt}\left(\int_{\text{system}} \vec{F} \cdot \vec{X}\right)$. That the principal stress directions must rotate is explained by first noting that the existence of $\dot{v}$ implies the existence of $\dot{\phi}$ and $\dot{G}$. Since Equation (28) shows that $\psi = \psi(\phi, G)$, then if ϕ and G change during the motion, ψ may also change. But if the same material which initially deforms at the onset of motion is to be the only material deforming during subsequent motion, then $\dot{\psi} = 0$. The only way this can occur is for the principal stress directions to rotate. Associated with this rotation rate is the development of a shear stress rate, $\dot{\sigma}_{yz}$. During an actual test this shear stress rate would have to be sustained by the testing apparatus. In the following the apparatus is assumed capable of adopting to the required loading.

For purposes of illustration consider the change in the principal stress directions that occurs in a small time interval Δt after motion begins. Retaining only first order terms in Δt, the Mohr stress circle for the yz plane is shown in Figure 8. The principal stresses after an increment of time, Δt, are consequently $\sigma_C + \sigma_L + \dot{\sigma}_C \Delta t$, σ_L, σ_L, while the rate at which the principal stresses rotate is

$$\dot{\alpha} = \frac{\sigma_{yz}}{\sigma_C} \tag{34}$$

The condition that these principal stresses continue to satisfy the yield criterion is the same as given by Equation (17) or

$$\dot{\sigma}_C = -2\left[\frac{\sin\phi}{1 - \cos\phi}\ \frac{\partial c}{\partial v} + (c - \sigma_L)\ \frac{\cos\phi}{(1 - \sin\phi)^2}\ \frac{\partial \phi}{\partial v}\right] \dot{v} \tag{35}$$

By differentiating Equation (28) with respect to time and subsequently setting $\dot{\psi}$ equal to $-\dot{\alpha}$ from Equation (34) leads to

$$\frac{2\dot{\sigma}_{yz}}{\sigma_C} \sin 2\psi = \dot{\phi} \cdot \left[\frac{\cos\phi\ (3G - 2 + G\cos 2\psi)}{2 - G\ (1 + \sin\phi)}\right] + \dot{G}\left[\frac{(1 + \sin\phi)(3 + \cos 2\psi)}{2 - G\ (1 + \sin\phi)}\right] \tag{36}$$

The terms ϕ, U, and σ_o are functions of v so that from Equation (5) it is seen that G may be regarded as a function of v and σ or for the triaxial test v and $\sigma_L + \frac{\sigma_C}{3}$ so that

$$\dot{G} = \frac{\partial G}{\partial v} \dot{v} + \frac{1}{3} \frac{\partial G}{\partial \sigma} \dot{\sigma}_C \tag{37}$$

where

$$\frac{\partial G}{\partial v} = \alpha \frac{\partial^2 U}{\partial v^2} \cdot \frac{2 \sin\phi \, (\sigma_o - \sigma_C/3 - \sigma_L)}{3 \, (1 + \sin\phi)(\sigma_o - \sigma_C/3 - \sigma_L + \alpha \frac{\partial U}{\partial v})^2}$$

$$- \frac{\partial \sigma_o}{\partial v} \alpha \frac{\partial U}{\partial v} \frac{2 \sin\phi}{3(1 + \sin\phi)(\sigma_o - \sigma_C/3 - \sigma_L + \alpha \frac{\partial U}{\partial v})^2}$$

$$+ \frac{\partial \phi}{\partial v} \alpha \frac{\partial U}{\partial v} \cdot \frac{2 \cos\phi}{3(1 + \sin\phi)^2(\sigma_o - \sigma_C/3 - \sigma_L + \alpha \frac{\partial U}{\partial v})} \tag{38a}$$

$$\frac{\partial G}{\partial v} = \alpha \frac{\partial U}{\partial v} \cdot \frac{2 \sin\phi}{3(1 + \sin\phi)(\sigma_o - \sigma_C/3 - \sigma_L + \frac{\partial G}{\partial \sigma})^2} \tag{38b}$$

and

$$\dot{\phi} = \frac{\partial \phi}{\partial v} \cdot \dot{v} \tag{39}$$

The external loading in this case does work on the system at a rate given by

$$\int_{\text{system}} \vec{F} \cdot \dot{\vec{X}} = \pi R^2 \sigma_C \dot{Z} + \pi R^2 H \frac{\sigma_L}{\cos\psi} \frac{\dot{v}}{v} \tag{40}$$

The quantities σ_L, H, ψ, and $\dot{Z}$ in Equation (40) are constant and hence the measure which determines the actual flow field becomes

$$\frac{d}{dt} \int_{\text{system}} \vec{F} \cdot \dot{\vec{X}} = \pi R^2 \dot{\sigma}_C \dot{Z} + \pi R^2 H \frac{\sigma_L}{\cos\psi} \left(\frac{\dot{v}}{v} \right)^{\cdot} + \pi R^2 \dot{\sigma}_{yz} \dot{Y} \tag{41}$$

The third term is present on the right hand side of Equation (41) since the principal stress axes rotate once motion begins. All of the quantities appear-

ing in Equation (41) have been evaluated except $\dot{(\dot{v}/v)}$ which may be found by differentiating Equation (33) divided by v with respect to time to obtain

$$\dot{\left(\frac{\dot{v}}{v}\right)} = 0 \tag{42}$$

Equations (35), (42), (36) and (32) may now be substituted into Equation (41) to obtain

$$\frac{d}{dt}\int_{system} \vec{F} \cdot \dot{\vec{X}} = \pi R^2 Z \left(\frac{\dot{Z}}{Z}\right)^2 S^{**} \tag{43}$$

where

$$S^{**} = S^{**}(v, \sigma_L)$$

$$= \frac{Z}{H} \cdot \frac{v \cdot \cos 2\psi}{\cos\psi} \left[-2\left\{\frac{\sin\phi}{1-\cos\phi}\frac{\partial c}{\partial v} + (c-\sigma_L)\frac{\cos\phi}{(1-\sin\phi)^2}\frac{\partial \phi}{\partial v}\right\}\right.$$

$$-\left\{\frac{\tan 3\psi}{\sin 2\psi} \cdot \frac{(c-\sigma_L)\sin\phi}{1-\sin\phi}\right\} \cdot \left\{\left(\frac{\cos\phi\,[3G - 2 + G\cos 2\psi]}{2 - G\,[1+\sin\phi\,]}\right)\frac{\partial \phi}{\partial v}\right.$$

$$+ \left(\frac{[1+\sin\phi][3+\cos 2\psi]}{2 - G\,[1+\sin\phi]}\right)\left(\frac{\partial G}{\partial v} - \frac{2}{3}\frac{\partial G}{\partial \sigma}\left[\frac{\sin\phi}{1-\cos\phi}\frac{\partial c}{\partial v}\right.\right.$$

$$\left.\left.\left.\left. + \frac{\{c-\sigma_L\}\cos\phi}{\{1-\sin\phi\}^2}\frac{\partial \phi}{\partial v}\right]\right)\right\}\Bigg] \tag{44}$$

The function S^{**} is similar to S^{*} in that on consideration of a specified material both functions may be determined if v and σ_L are known. For this second solution the value of H, the constant layer thickness, has not yet been specified. If S^{**} is greater than zero the largest possible value of H gives the smallest S^{**}. Therefore S^{**} can be minimized by setting

$$H = Z\cos\psi - 2R\sin\psi \tag{45}$$

when S^{**} is greater than zero. Should S^{**} be less than zero then the smallest possible value of H is the one which minimizes S^{**}. Consequently

$$H = 0 \tag{46}$$

when S^{**} is negative. The modes of motion for each of the above possibilities

are shown in Figure 9. It should be noted also that when S^{**} is negative and H approaches zero, S^{**} approaches an unbounded negative number. As no parameter exists in the first solution such as H, which is arbitrary ($0 \leq H \leq Z \cos\psi - 2R \sin\psi$), S^{*} is bounded. Consequently when S^{**} is negative the solution depicted in Figure 9b must be the actual solution. When S^{**} is positive then its minimum value must be compared to S^{*} to determine the actual mode of deformation.

Clearly, the above solutions may not be the only solutions so that the comparisons given here really only pertain to determining which which of the considered solutions is likely to be the actual solution.

Numerical Solution

In order to demonstrate predictions which the preceding results yield a numerical example is presented. Several functions must be given explicitly in order to make this evaluation. Published experimental results [6] for Leighton Buzzard sand were used in order to select appropriate input for the calculations. The following choices are consistent with the experimental results and theoretical requirements of Equations (6):

$$c = 0 \tag{47.a}$$

$$\phi = \phi_o + \frac{\partial \phi}{\partial v} (v - v_o) \tag{47.b}$$

$$\sigma_o = - (\frac{v_1 - v}{v - v_o}) M \tag{47.c}$$

$$\alpha U = \alpha K \int_{v_1}^{v} \sigma_o dv \tag{47.d}$$

where

$$\phi_o > 0 \tag{48.a}$$

$$\frac{\partial \phi}{\partial v} < 0 \tag{48.b}$$

$$v_o < v < v_1 \tag{48.c}$$

$$M > 0 \tag{48.d}$$

$$1 > K > 0 \tag{48.e}$$

$$0 < \alpha < 1 \tag{48.f}$$

From Equations (47) and (48) it can be determined that

$$\alpha U = \alpha KM \left[- (v_1 - v) + (v_1 - v_o) \ln \left(\frac{v_1 - v_o}{v - v_o} \right) \right] \tag{49.a}$$

$$\alpha \frac{\partial U}{\partial v} = - \alpha KM \left(\frac{v_1 - v}{v - v_o} \right) \tag{49.b}$$

$$\alpha \frac{\partial^2 U}{\partial v^2} = \alpha KM \frac{(v_1 - v_o)}{(v - v_o)^2} \tag{49.c}$$

$$\frac{\partial \sigma_o}{\partial v} = + \frac{(v_1 - v_o)}{(v - v_o)^2} \; M \tag{49.d}$$

From the experimental results of [6] the following magnitudes were selected for the material parameters of Equations (48)

$$\phi_o = 0.686 \text{ radians} = 39.4^o \tag{50.a}$$

$$\frac{\partial \phi}{\partial v} = - 0.100 \text{ radians} - \text{lb./in.}^3 \tag{50.b}$$

$$v_o = 16.08 \text{ in.}^3/\text{lb.} \tag{50.c}$$

$$v_1 = 19.00 \text{ in.}^3/\text{lb.} \tag{50.d}$$

$$M = 129 \text{ lbs./in.}^2 \tag{50.e}$$

$$\alpha K = 0.1 \tag{50.f}$$

The initial homogeneous state of the sample for the calculations of the numerical example is described by

$$v = 16.88 \text{ in.}^3/\text{lb.} \tag{51.a}$$

$$\sigma_L = - 50 \text{ lbs./in.}^2 \tag{51.b}$$

The preliminary evaluations needed for determination of both S^{*} and S^{**} are

$$\phi = 34.7^{o} \quad \text{from Eq. (47.b)} \quad (52.a)$$

$$\sigma_{o} = -343 \text{ lbs./in.}^{2} \quad \text{from Eq. (47.c)} \quad (52.b)$$

$$\alpha U = + 21.5 \text{ lb.-in./in.} \quad \text{from Eq. (49.a)} \quad (52.c)$$

$$\frac{\partial \sigma_{o}}{\partial v} = + 592 \text{ lb.}^{2}/\text{in.}^{5} \quad \text{from Eq. (49.d)} \quad (52.d)$$

$$\alpha \frac{\partial U}{\partial v} = - 34.3 \text{ lb./in.}^{2} \quad \text{from Eq. (49.b)} \quad (52.e)$$

$$\alpha \frac{\partial^{2} U}{\partial v^{2}} = 59.2 \text{ lb.}^{2}/\text{in.}^{5} \quad \text{from Eq. (49.c)} \quad (52.f)$$

$$\sigma_{c} = -132 \text{ lbs./in.}^{2} \quad \text{from Eqs. (9), (47.a) (52.a)} \quad (52.g)$$

$$\sigma = -94 \text{ lbs./in.}^{2} \quad \text{from Eqs. (1), (52.g)} \quad (52.h)$$

$$G = + 0.0293 \quad \text{from Eqs. (5), (52.e) (52.b), (52.h)} \quad (52.i)$$

$$\frac{\partial G}{\partial v} = + 0.0140 \text{ lb./in.}^{3} \quad \text{from Eqs. (38.a), (52.f) (52.b), (52.g), (52.e) (52.d)} \quad (52.j)$$

$$\frac{\partial G}{\partial \sigma} = - 1.038 \times 10^{-4} \text{ in.}^{2}/\text{lb.} \quad \text{from Eqs. (38.b), (52.c) (52.b), (52.g)} \quad (52.k)$$

For the first mode of deformation considered

$$\dot{v} = - 35.4 \left(\frac{\dot{Z}}{Z}\right) \quad \text{from Eq. (18)} \quad (53.a)$$

$$\sigma_{c} = - 1570 \left(\frac{Z}{Z}\right) \quad \text{from Eq. (17)} \quad (53.b)$$

$$\dot{R} = - 1.55 \, R \left(\frac{\dot{Z}}{Z}\right) \quad \text{from Eq. (19)} \quad (53.c)$$

$$\ddot{R} = - 11.78 \, R \left(\frac{\dot{Z}}{Z}\right)^{2} \quad \text{from Eq. (20)} \quad (53.d)$$

Substituting the above into Equation (16) yields

$$\frac{d}{dt}\int_{system} \vec{F} \cdot \dot{\vec{X}} = \pi R^2 Z \, (\dot{Z}/Z)^2 \; (+\,88) \qquad (54)$$

So that from Equation (21)

$$S^{*} = +\,88 \qquad (55)$$

For the second mode of deformation considered:

$$\psi = 60.4^{o} \qquad \text{from Eq. (28)} \qquad (56.a)$$

$$\dot{v} = -\,17.48\,\frac{Z}{H} \qquad \text{from Eq. (33)} \qquad (56.b)$$

$$\dot{\sigma}_{c} = -\,774\,\frac{\dot{Z}}{H} \qquad \text{from Eq. (35)} \qquad (56.c)$$

$$\dot{\phi} = +\,1.748\,\frac{\dot{Z}}{H} \qquad \text{from Eq. (39)} \qquad (56.d)$$

$$\dot{G} = -\,0.217\,\frac{\dot{Z}}{H} \qquad \text{from Eq. (37)} \qquad (56.e)$$

$$\dot{\sigma}_{yz} = +\,142\,\frac{\dot{Z}}{H} \qquad \text{from Eq. (36)} \qquad (57.f)$$

$$\dot{Y} = -\,1.755\,\frac{\dot{Z}}{H} \qquad \text{from Eq. (32)} \qquad (58.g)$$

Substituting Equations (42) and (56) into Equation (41) yields

$$\frac{d}{dt}\int_{system} \vec{F} \cdot \dot{\vec{X}} = \pi R^2 Z \, (\dot{Z}/Z)^2 \; \left(-\,1023\,\frac{Z}{H}\right) \qquad (59)$$

so that from Equation (43)

$$S^{**} = -\,1023\,\left(\frac{Z}{H}\right) \qquad (60)$$

From the remarks previously made concerning the effect of the sign of S^{**}, the actual mode of deformation of the specimen in this numerical example is the one shown in Figure 9b. There is of course a geometric requirement that the height Z of the sample be large enough to allow a slip plane to form. That is, for the second mode of deformation to occur

$$\frac{Z}{R} > 2 \tan\psi = 3.52 \tag{61}$$

It may be noted from the calculations that the first mode of deformation is stable as S^* is positive, primarily because the rate at which the radius increases is enough to offset the decreasing σ_c.

The above numerical results indicate a behavior which is consistent with observed soil tests. The reader should note that while this theory predicts a flow similar to that shown in Figure 9b, it must be noted that, in practice, a rubber membrane surrounds the sample and that the finite size of the grains prevents H from approaching zero. Such stabilizing effects may be responsible for the observed experimental result that the flow shifts from plane to plane as the motion proceeds.

Bibliography

1. J. B. Weidler and P. R. Paslay, "An Analytical Description of the Behavior of Granular Media" to be submitted for publication.

2. R. T. Shield, "On Coulomb's Law of Failure in Soils", Journal of the Mechanical and Physics of Solids, 1955, vol. 4, pp. 10-16.

3. D. C. Drucker, R. E. Gibson, and D. J. Henkel, "Soil Mechanics and Work-Hardening Theories of Plasticity," Transactions of the American Society of Civil Engineers, 1957, vol. 122, pp. 338-346.

4. A. W. Jenike and R. T. Shield, "On the Plastic Flow of Coulomb Solids Beyond Original Failure", Journal of Applied Mechanics, 1959, vol. 29, pp. 599-602.

5. D. C. Drucker, "On Uniqueness in the Theory of Plasticity", Quarterly of Applied Mathematics, 1956, vol. 14, pp. 35-42.

6. K. H. Roscoe, A. N. Schofield and A. Thurairajah, "An Evaluation of Test Data for Selecting a Yield Criterion for Soils", ASTM STP 361, Laboratory Shear Testing of Soils, 1964, pp. 111-128.

FIGURE CAPTIONS

Figure 1 - Coulomb-Mohr Loading Surface in Principal Stress Space

Figure 2 - Intersection of Coulomb-Mohr Loading Surface with π Plane for $\sigma = \frac{1}{3}(\sigma_1 + \sigma_2 + \sigma_3) \leq c$

Figure 3 - Intersection of Loading Surface and Plane in Principal Stress Space Which Includes the σ_3 axis and is Parallel to the Vector $\vec{i} + \vec{j} + \vec{k}$

Figure 4 (a) - Same Section as Figure 3 showing direction for Deformation Rate Vector, $d_1\vec{i} + d_2\vec{j} + d_3\vec{k}$

(b) - π Plane Showing the Fan of Possible Projections of $d_1\vec{i} + d_2\vec{j} + d_3\vec{k}$ onto the Plane

Figure 5 - Triaxial Test Sample Showing Applied Stresses σ_C, σ_L and Dimensions

Figure 6 - Deformation of Shearing Layer

Figure 7 - Mohr Strain Circle for Shearing Layer

Figure 8 - Mohr Stress Circle for Time $t + \Delta t$ in the yz Plane for Shearing Layer

Figure 9 - Modes of Deformation for Shearing Solution

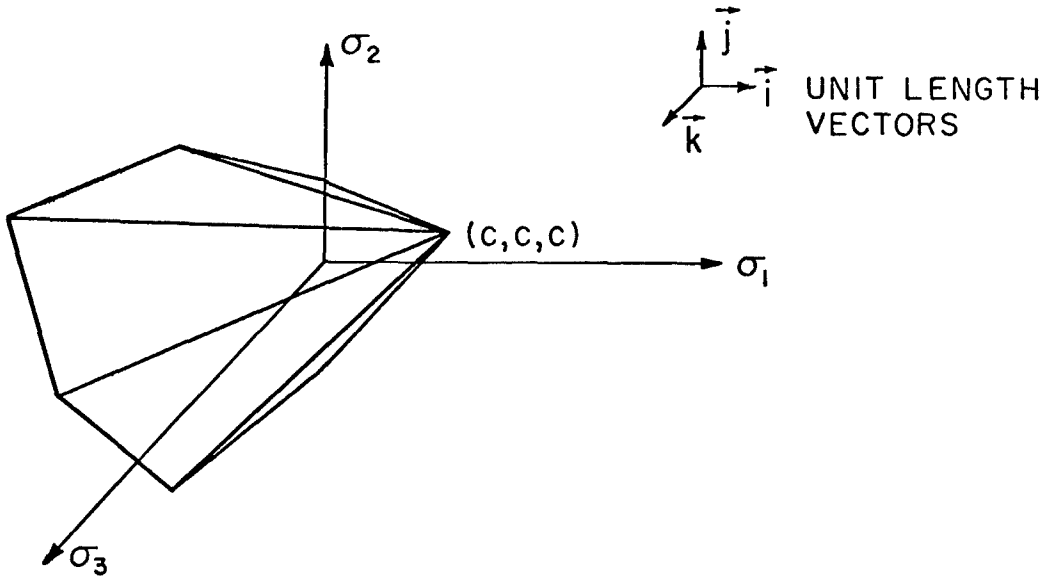

FIG. 1 COULOMB - MOHR LOADING SURFACE IN PRINCIPAL STRESS SPACE

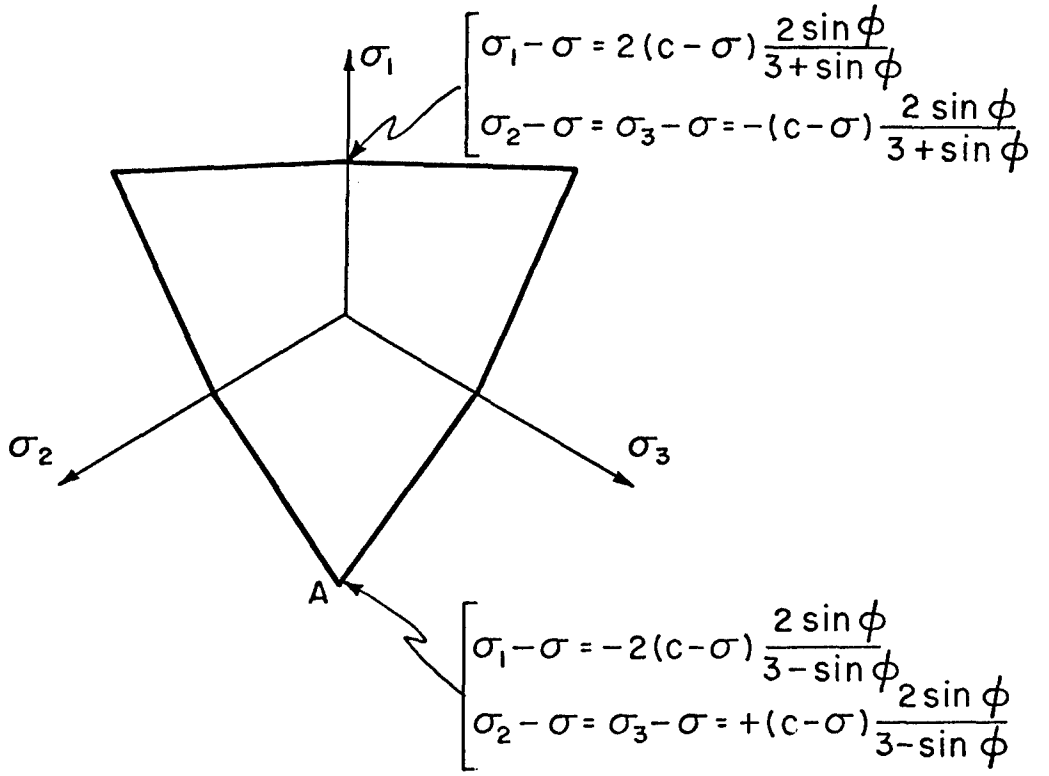

FIG. 2 INTERSECTION OF COULOMB - MOHR LOADING SURFACE WITH π PLANE FOR $\sigma = \frac{1}{3}(\sigma_1 + \sigma_2 + \sigma_3) \leq C$.

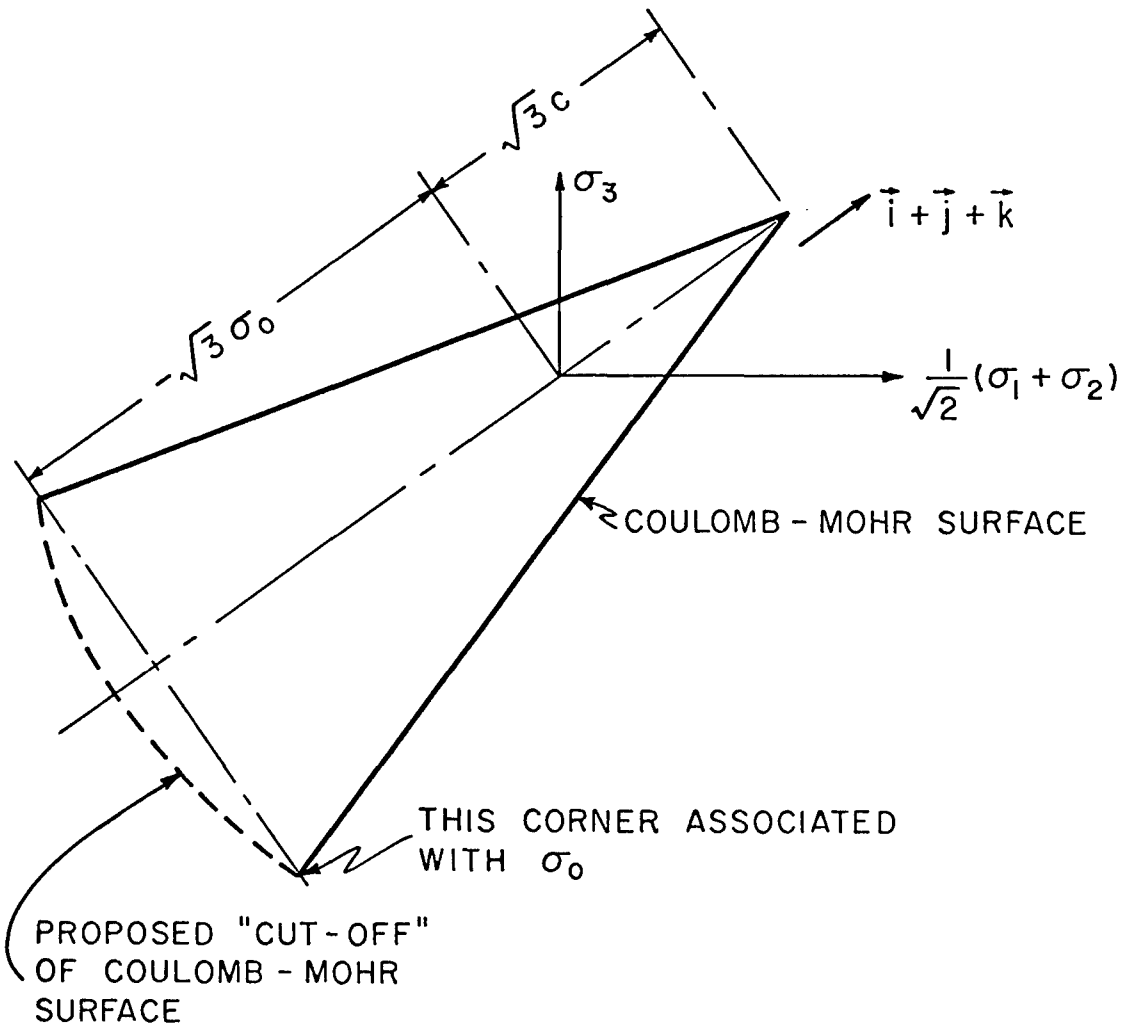

FIG. 3 INTERSECTION OF LOADING SURFACE AND PLANE IN PRINCIPAL STRESS SPACE WHICH INCLUDES THE σ_3 AXIS AND IS PARALLEL TO THE VECTOR $\vec{i}+\vec{j}+\vec{k}$.

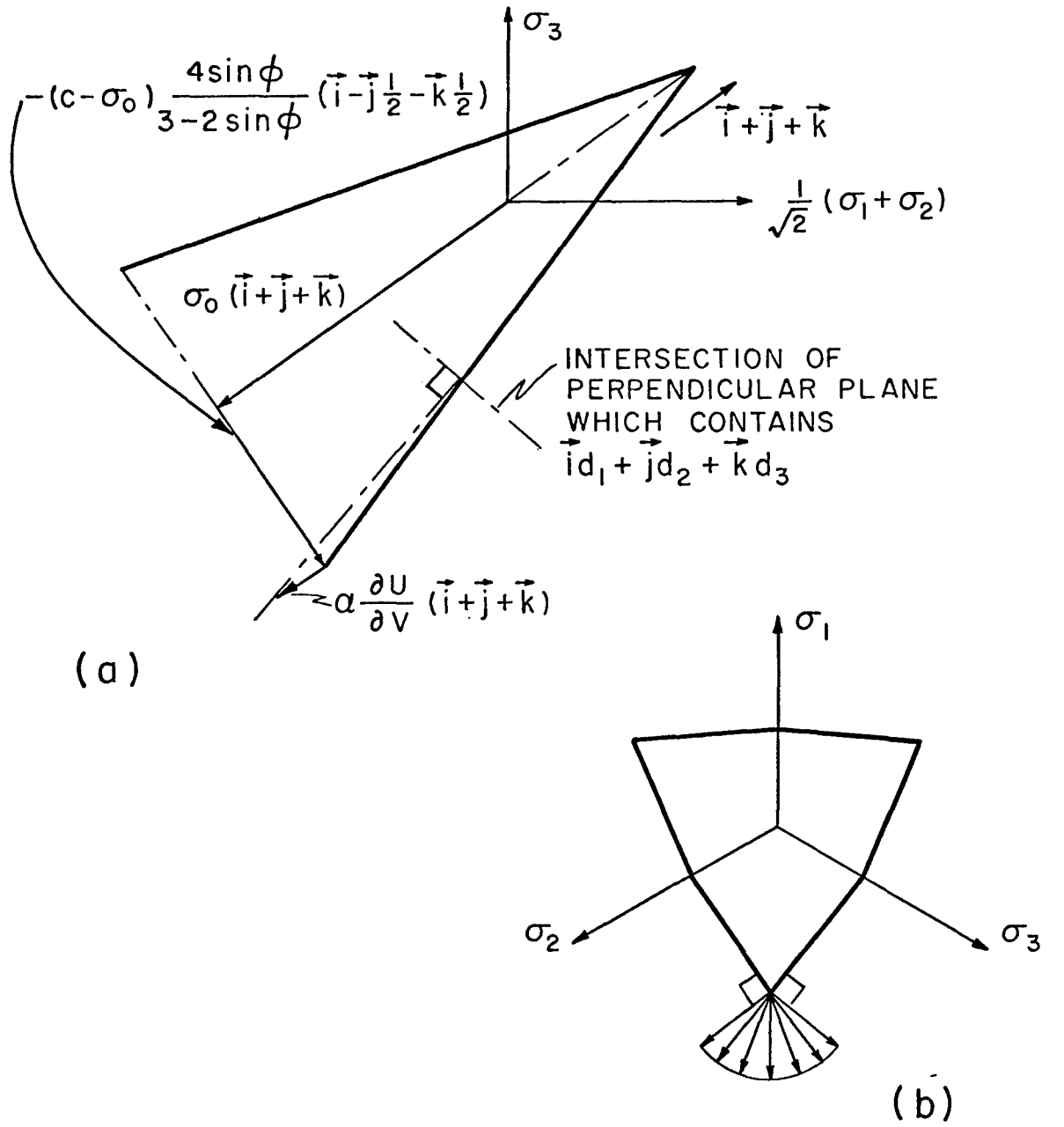

FIG. 4 (a) SAME AS FIG. 3 SHOWING DIRECTION FOR DEFORMATION RATE VECTOR, $\vec{i}d_1+\vec{j}d_2+\vec{k}d_3$, WHEN $\frac{\partial U}{\partial V}$, $\sigma_0 < 0$.

(b) $-\pi$ PLANE SHOWING THE FAN OF POSSIBLE PROJECTIONS OF $\vec{i}d_1+\vec{j}d_2+\vec{k}d_3$ ONTO THE PLANE.

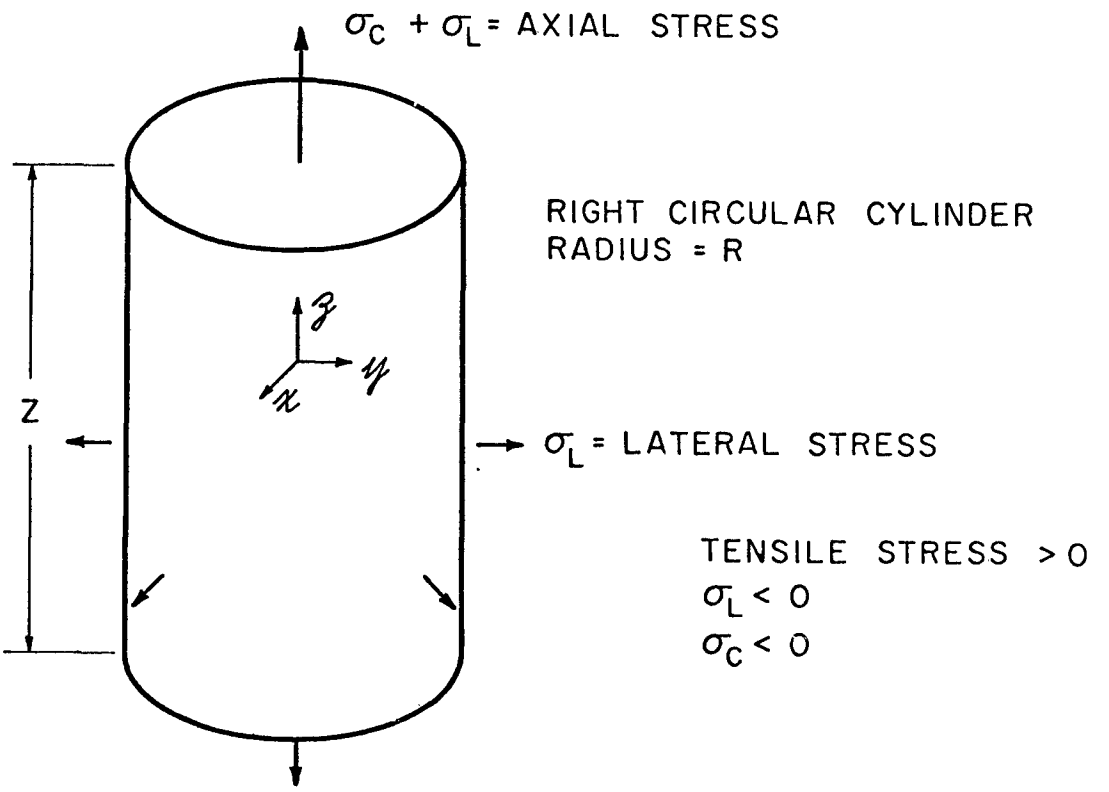

FIG.5 TRIAXIAL TEST SAMPLE SHOWING APPLIED STRESSES σ_C , σ_L AND DIMENSIONS.

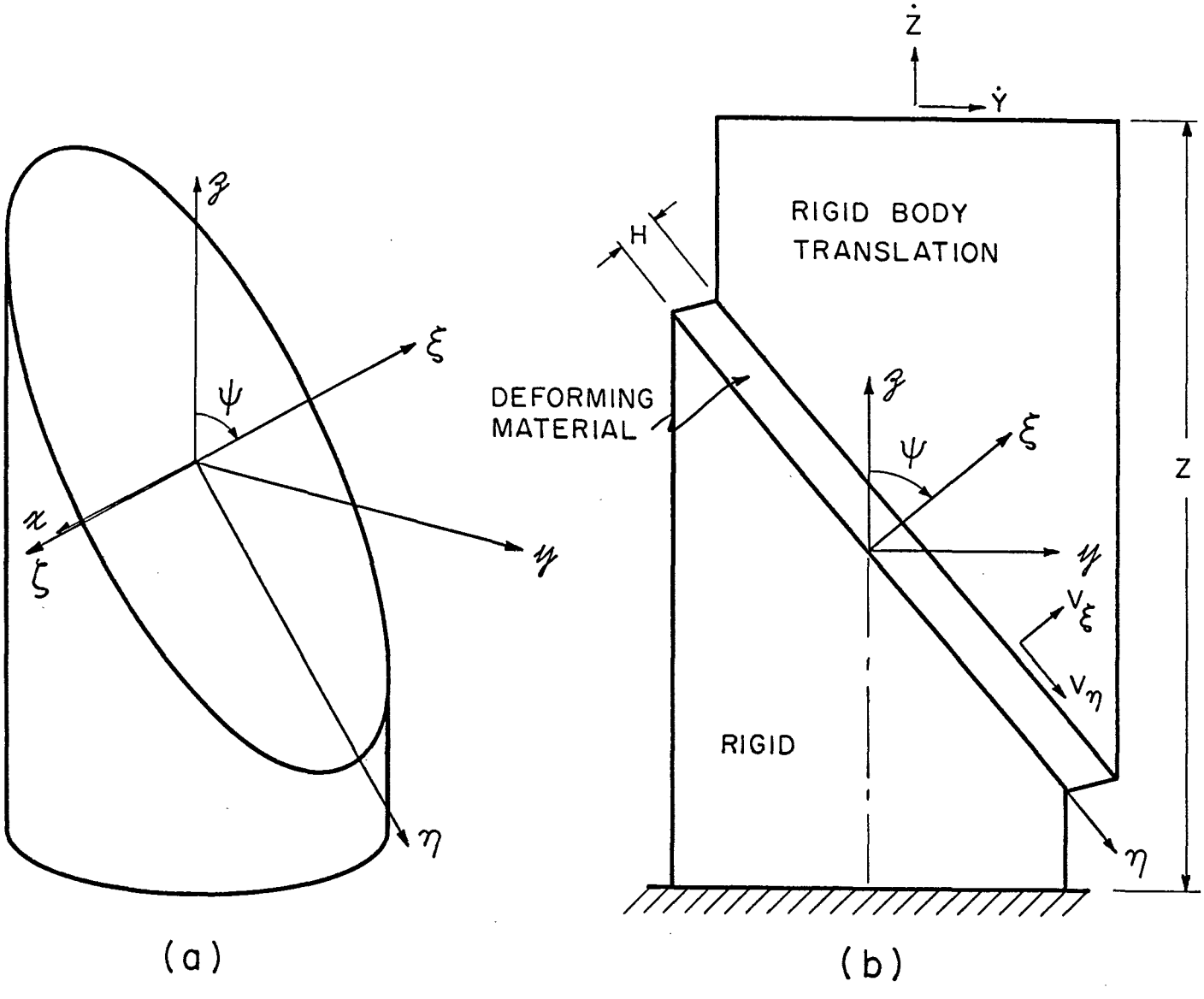

FIG. 6 DEFORMATION OF SHEARING LAYER.

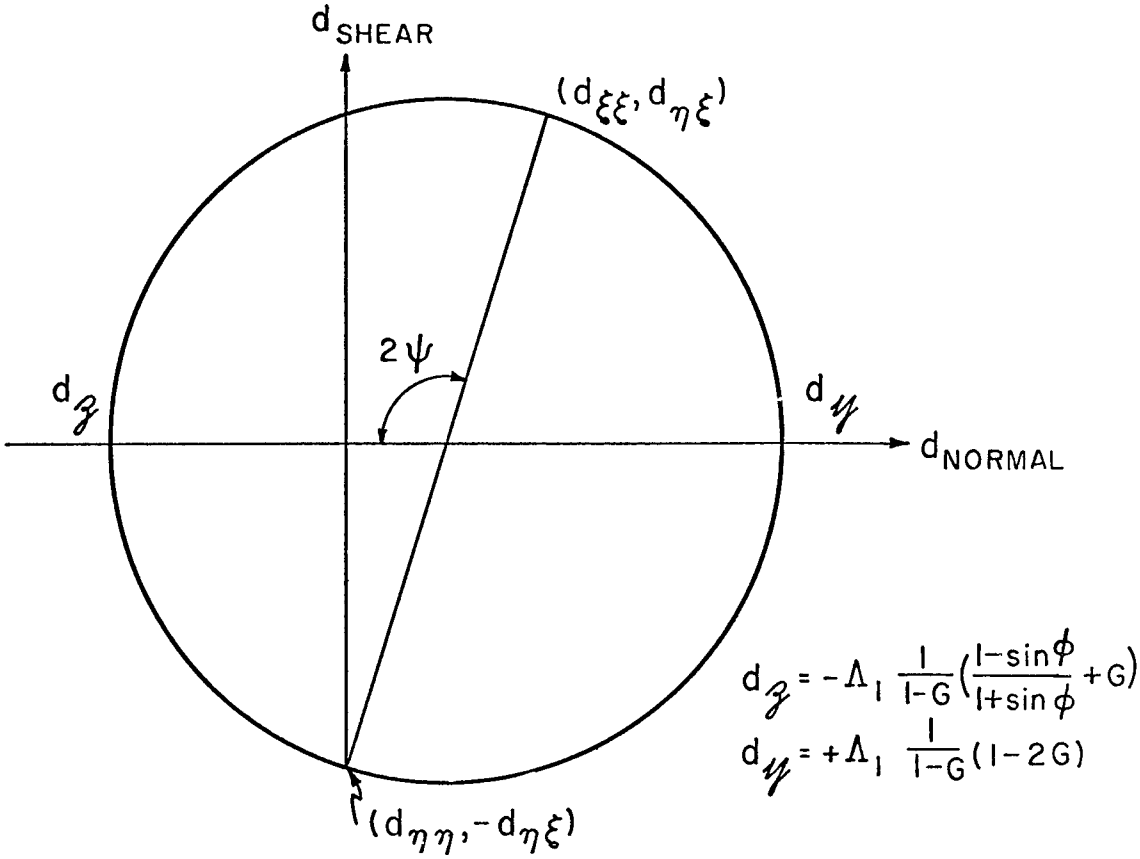

FIG. 7 MOHR STRAIN CIRCLE FOR SHEARING LAYER

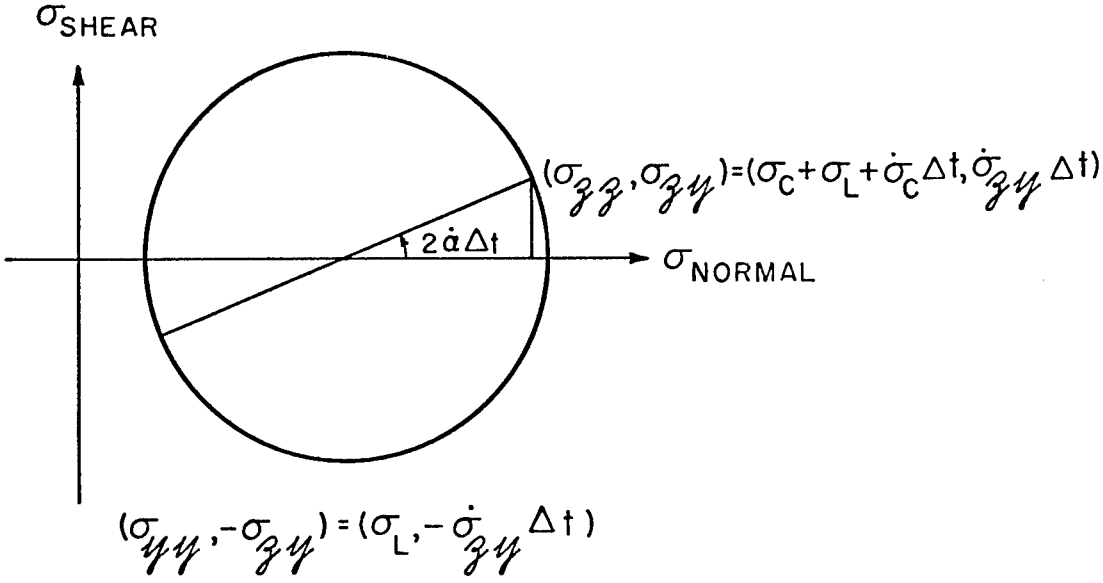

FIG. 8 MOHR STRESS CIRCLE FOR TIME $t + \Delta t$ IN THE yz PLANE FOR SHEARING LAYER.

$s^{**}>0$

(a)

$s^{**}<0$

(b)

FIG. 9 MODES OF DEFORMATION FOR SHEARING SOLUTION.